INSTITUTE OF PHYSICS PUBLISHING NANOTECHNOLOGY
Nanotechnology **18** (2007) 044018 (8pp) doi:10.1088/0957-4484/18/4/044018

Conductance of redox-active single molecular junctions: an electrochemical approach

Zhihai Li[1], Ilya Pobelov[1], Bo Han[1], Thomas Wandlowski[1,4], Alfred Błaszczyk[2,5] and Marcel Mayor[2,3]

[1] Institute of Bio- and Nanosystems IBN 3 and cni—Center of Nanoelectronic Systems for Information Technology, Research Center Jülich GmbH, D-52425 Jülich, Germany
[2] Institute for Nanotechnology, Research Center Karslruhe GmbH, PO Box 3640, D-76021 Karlsruhe, Germany
[3] Department of Chemistry, University of Basel, St Johanns-Ring 19, CH-4056, Basel, Switzerland

E-mail: th.wandlowski@fz-juelich.de

Received 19 August 2006, in final form 27 October 2006
Published 12 December 2006
Online at stacks.iop.org/Nano/18/044018

Abstract
The conductance of molecular junctions formed of N,N'-bis(n-thioalkyl)-4,4′-bipyridinium bromides or alkanedithiols between a gold (Au) scanning tunnelling microscope tip and a Au(111)-(1 × 1) electrode has been studied at electrified solid/liquid interfaces. A statistical analysis based on large sets of individual current–distance traces was applied to obtain the electrical conductance of single junctions. The one-electron reduction of the viologen moiety from the dication V^{2+} to the radical cation state $V^{+\cdot}$ gives rise to a 50% increase of the junction conductance. Increasing the length of the alkyl spacer units leads to a tunnelling decay constant $\beta_{CH2} = 5.9$–$6.1\ nm^{-1}$. This value is significantly lower than $\beta_{CH2} = 8.2\ nm^{-1}$ estimated for molecular junctions of alkanedithiols. The difference is attributed to conformational changes within the two junctions. The contact conductance was estimated to 10 μS.

M Supplementary data files are available from stacks.iop.org/Nano/18/044018

(Some figures in this article are in colour only in the electronic version)

1. Introduction

As the miniaturization of electronic components approaches the nanometre scale, new concepts for tailoring the structure and functionality and new fabrication strategies are essential. A particularly fascinating topic deals with the charge transfer in (single) molecular redox systems [1–7]. The construction of metal/molecule/metal junctions with device-like functions, such as switching or rectification, requires a source and a drain electrode as well as one or more addressable localized electronic levels. The role of source and drain may be represented by the conducting tip of a scanning probe microscope in combination with a tailored substrate or a pair of nanoelectrodes separated by molecular-scale gaps [2–7]. Operating the experiment in an electrochemical environment has the advantage that two potential differences can be controlled separately: the bias voltage between two working electrodes (source, drain) as well as the potential between each working electrode and a reference electrode. The latter may be considered as an 'electrolyte gate'. The field in the electrochemical double layer (EDL), $\sim 10^9\ V\ m^{-1}$, is close to the gate field required to significantly change the current through a single molecular junction, according to first principles calculations by di Ventra [8].

The concept of electrochemical gating has been applied to control charge transport in conducting polymer films [9], nanojunctions [10], metal oxide semiconductors [11], carbon nanotubes [12, 13] and redox molecules [14–26]. The

[4] Author to whom any correspondence should be addressed.
[5] On leave from: Faculty of Commodity Science, Aleja Niepodległości 10, 60-967 Poznań, Poland.

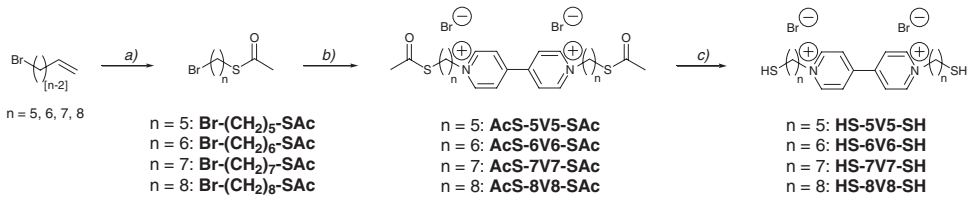

Scheme 1. Synthesis of HS-*n*V*n*-SH: (a) CH_3COSH, 1,1′-azo-bis-(cyclohexanecarbonitrile), toluene, reflux, 1 h; (b) 4,4′-bipyridine, DMF, 110 °C, 24 h; (c) AcBr, MeOH, −78 °C to room temperature, argon atmosphere, 3 h.

first examples for switching and rectification employing single molecular junctions under electrochemical conditions were reported for Fe(III) protoporphyrin-IX [14], directly bound or alkylviologens tethered to a gold substrate via gold nanoparticles [15–17], metal proteins [18, 19], perylene tetracarboxylic diimide [20], functionalized oligo-(phenylene) ethynylene derivatives [21], and transition metal complexes [22–24] as well as nanometre-sized junctions with oligothiophene [25] or oligoaniline molecules [26, 27]. These experiments demonstrate the unique abilities of redox molecules for tuning the electron transport in nanoscale two- and three-terminal junctions.

We report in this paper on the potential-dependent single molecule conductance of *N*,*N*′-bis(*n*-thioalkyl)-4,4′-bipyridinium bromide (HS-*n*V*n*-SH, $n = 5$ to 8) chemically bound to two gold electrodes in an electrochemical environment. Our approach involves the repeated formation and breaking of molecular junctions between a gold STM tip (Au(T)) and a Au(111)-(1 × 1) substrate (Au(S)). This technique was pioneered by Tao *et al* [28] and Haiss *et al* [16]. HS-*n*V*n*-SH molecules are composed of a redox-active viologen centre attached to flexible alkyl spacer units and two terminal thiol anchor groups. The viologen group may exist in three different states depending on the applied electrode potential: as the dication V^{2+} in the stable oxidized form, and in the two electron-rich forms, the radical cation $V^{+\cdot}$ and the neutral $V^{\cdot}$ species [29]. They have been incorporated as backbone components in self-assembled monolayers (see [30] and references cited in [17]), in a nanometre-scale electronic switch [15] and in various functional materials [31]. The self-assembly and redox-functionality of alkylthiol viologens on gold electrodes was investigated by cyclic voltammetry [30, 32, 33], use of a quartz crystal microbalance [33], infrared and Raman spectroscopy [17, 34, 35], electroreflectance [33], and *ex situ* scanning tunnelling microscopy (STM) and spectroscopy (STS) [15–17, 35].

With the present study we aim at exploring the single molecule conductance of Au(T)/HS-*n*V*n*-SH/Au(S)[6] junctions with viologen derivatives of variable alkyl spacer length in aqueous electrolyte under potential control. The project extends our previously reported experiments with HS-6V6-SH [17]. The conductance characteristics of redox-active viologen-based molecular wires will be compared with junctions composed of 'insulating' alkandithiols HS-C_m-SH.

[6] As a convention of this paper, all molecules in junctions are presented as they are provided in solution. The terminal hydrogen atoms may be removed upon formation of S–Au bonds in the junctions.

2. Experimental details

2.1. Synthesis

The synthesis of viologen derivatives comprising terminally sulfur-functionalized alkyl chains of various length (HS-*n*V*n*-SH; $n = 5, 6, 7, 8$) is displayed in scheme 1. It mainly follows the procedure already reported for the synthesis of HS-6V6-SH [17] and is only discussed briefly. However, experimental protocols and analytical data of all HS-*n*V*n*-SH target compounds and their precursors are provided as supplementary data (available at stacks.iop.org/Nano/18/044018).

As displayed in scheme 1, alkyl precursors of various length comprising bromides and acetylthiol groups on opposite endings have been obtained from the corresponding bromo-*n*-alkenes. Nucleophilic substitution of the terminal bromides of the alkyl precursors by both nitrogen atoms of bipyridine provided the acetyl protected target compounds AcS-*n*V*n*-SAc. Subsequent hydrolysis with HBr afforded the viologen derivatives comprising terminal *n*-alkylthiol spacers HS-*n*V*n*-SH. The identity and purity of the target compounds and their precursors are confirmed by ^{1}H and ^{13}C-NMR spectroscopy, MS spectrometry and elemental analysis.

The alkanedithiols (HS-C_m-SH) pentanedithiol (C_5), hexanedithiol (C_6), octanedithiol (C_8), nonanedithiol (C_9) and decanedithiol (C_{10}) were purchased from Alpha Aesar (p.a. 99%) and used without further purification.

2.2. Electrolyte solutions and electrochemical measurements

The electrolyte solutions were prepared with Milli-Q water (18 MΩ, 2 ppb TOC), $KClO_4$ (Fluka puriss. p.a., twice recrystallized from ultrapure water), KOH (suprapure, Merck) and ethanol (p.a. KMF). All electrolytes were deaerated with 5 N argon before and during the electrochemical experiments. The measurements were carried out at (20.0 ± 0.5) °C. The glassware was cleaned in caroic acid followed by extended rinsing with Milli-Q water. The electrochemical measurements were performed with an Autolab PGSTAT30 working station employing a home-built three-electrode glass cell. The counter electrode was a platinum wire, and a saturated calomel electrode (SCE) served as reference. All potentials in this paper are quoted with respect to this electrode.

2.3. Electrode and sample preparation

The Au(111) single crystals used in this work were massive cylinders of 4 mm height and 4 mm diameter (cyclic voltammetry), or 2 mm height and 10 mm diameter (STM). Before each experiment, the electrodes were annealed in a butane or hydrogen flame at bright red heat for about 10 min,

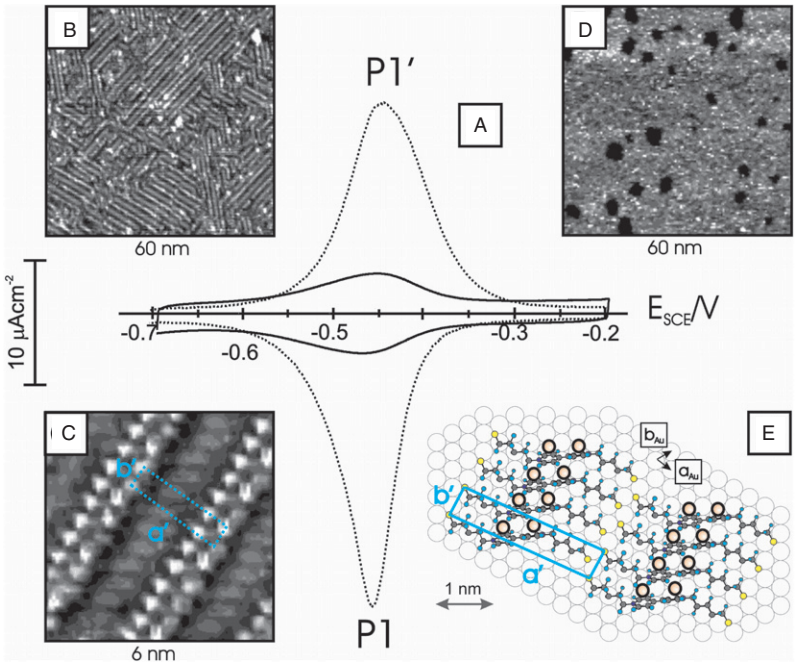

Figure 1. (A) Cyclic voltammogram of a Au(111)-(1 × 1) electrode in 0.05 M $KClO_4$, pH ∼ 7, modified with a low-coverage (solid line) and a high-coverage (dotted line) adlayer of HS-5V5-SH for the reversible one-electron oxidation/reduction between the viologen dication V^{2+} and the radical cation $V^{+\cdot}$ form. (B) Large scale *in situ* STM image of the low-coverage striped phase of HS-5V5-SH, $E_S = -0.25$ V, $E_{bias} = 0.10$ V, $i_T = 60$ pA; (C) high-resolution image of the striped phase, $E_S = -0.35$ V, $E_{bias} = 0.08$ V, $i_T = 40$ pA; (D) high-coverage adlayer of HS-5V5-SH, $E_S = -0.25$ V, $E_{bias} = 0.09$ V, $i_T = 60$ pA; (E) proposed packing model of the ordered striped phase.

and then cooled in an argon atmosphere. Island-free Au(111)-(1 × 1) surfaces were prepared by immersing of a flame-annealed Au(111)-(p × $\sqrt{3}$) electrode in 0.05 M HCl, followed by rinsing with copious amounts of Milli-Q water and drying in a stream of argon.

Low-coverage ordered adlayers of HS-*n*V*n*-SH were prepared by exposure of the Au(111)-(1 × 1) electrode at room temperature to 100 μM deoxygenated ethanolic solution of the respective viologen for 2 min and subsequent annealing in pure ethanol at 70 °C for 12 h. High-coverage monolayers of HS-*n*V*n*-SH were obtained by immersion of the gold substrate into 1 mM ethanolic solution followed by thermal annealing at 70 °C for 12 h. The alkanedithiol adlayers were prepared by contacting a Au(111)-(1 × 1) electrode with a 1 mM ethanolic solution for 10 min. The temperature treatment of all samples was carried out in closed, deoxygenated containers. After incubation the samples were removed from the respective solutions, rinsed with ethanol, carefully dried in a stream of argon, and subsequently mounted into the electrochemical or STM cell.

2.4. STM and STS measurements

The STM and STS measurements were carried out with freshly modified Au(111)-(1 × 1) electrodes in 0.05 M $KClO_4$, pH ∼ 7 adjusted with KOH, in a hermetically sealed container to prevent oxygen exposure of the samples, using a Molecular Imaging Pico Scanning Tunnelling Microscope. The STM tips were electrochemically etched tungsten or gold wires (0.25 mm diameter) coated with polyethylene. The electrochemical leakage current was typically ≪1 pA. A platinum wire served as a counter electrode. A carefully calibrated silver wire was employed as quasi-reference electrode. All STM experiments were performed at room temperature in constant current mode with tunnelling currents ranging between 3 and 200 pA.

Single molecular conductance experiments with Au(T)/HS-*n*V*n*-SH (HS-C_m-SH)/Au(S) junctions were carried out by current–distance measurements with *in situ* STM imaging [17]. Our approach represents a slight, but distinct, modification of two methods recently introduced by Tao [28] and Haiss [16]: a carefully coated (except at the very end) gold STM tip was brought to a present tunnelling position under feedback control, typically choosing a tunnelling current of 100 pA and a bias voltage $E_{bias} = (E_T - E_S)$ of 0.10 V. Subsequently, the feedback was switched off, and the tip approached at constant xy-position the viologen-(alkandithiol-) modified surface. The approach stopped 0.1 to 0.2 nm before reaching physical contact (=quantum point contact) with the substrate. After a dwelling time of 100 ms, sufficient to create molecular junctions between tip and substrate, the tip was retracted with a pulling rate of 2–4 nm s^{-1}. The corresponding current–distance trace was recorded. Finally, the feedback was switched on again. The cycle was repeated after stabilization. The statistical analysis of the single junction conductance characteristics was carried out with a data base of 500 up to 2000 individual traces. During these measurements, the surface was regularly inspected by *in situ* STM imaging.

3. Results and discussion

3.1. Cyclic voltammetry and in situ STM imaging

A typical cyclic voltammogram for a Au(111)-(1 × 1) electrode modified with two distinct concentrations of *N*,*N*′-bis(5-

Table 1. Unit cell parameters of the low-coverage striped phase of HS-*n*V*n*-SH on Au(111)-(1 × 1).

Viologen	a' (nm)[a]	b' (nm)[a]	α (deg)[a]	Γ (10^{-10} mol cm^{-2})	A (nm^2)
5V5	2.4 ± 0.3	0.50 ± 0.03	83 ± 3	1.4	1.2
	(2.5)	(0.5)	(83)	(1.3)	(1.2)
6V6	2.8 ± 0.3	0.50 ± 0.03	87 ± 8	1.2	1.4
	(2.8)	(0.5)	(84)	(1.2)	(1.4)
7V7	3.0 ± 0.3	0.50 ± 0.03	84 ± 5	1.1	1.5
	(3.0)	(0.5)	(84)	(1.1)	(1.5)
8V8	3.3 ± 0.3	0.50 ± 0.03	86 ± 7	1.0	1.6
	(3.3)	(0.5)	(85)	(1.0)	(1.6)
10V10	3.8 ± 0.5	0.50 ± 0.03	86 ± 4	0.88	1.9
	(3.9)	(0.5)	(86)	(0.85)	(1.9)

[a] The numbers in parentheses represent the model parameters.

thiopentyl)-4,4′-bipyridinium bromide in 0.05 M $KClO_4$, pH $\sim$ 7 is shown in figure 1(A). The low-coverage curve is represented by the solid line, the high-coverage trace by the dashed curve. The two peaks P1 ($E = -0.470$ V) and P1′ ($E = -0.450$ V) correspond to the reversible electron transfer between the viologen dication and the radical cation $V^{2+} \leftrightarrow V^{+\cdot}$ [17, 29]. The peak-to-peak separation is rather constant, and the peak heights scale linearly with scan rate. These observations indicate a fairly reversible process. The coverages were estimated to be $\Gamma_L(CV) = (1.2 \pm 0.2)\ 10^{-10}$ mol cm^{-2} for the low-coverage phase and $\Gamma_H(CV) = (3.8 \pm 0.2)\ 10^{-10}$ mol cm^{-2} for the high-coverage phase, respectively. The corresponding areas per molecule were estimated to be 1.38 and 0.44 nm^2. The latter points to a perpendicular or tilted viologen surface orientation. *In situ* STM images of the high-coverage phase of HS-5V5-SH are rather disordered and show characteristic monatomic deep holes (figure 1(D)). Similar results were obtained with high-coverage adlayers of the other HS-*n*V*n*-SH viologen adlayers. A highly ordered striped adlayer of planar oriented molecules [17] is formed at low coverages in $-0.70\ \text{V} \leqslant E \leqslant -0.20$ V, i.e. within the stability ranges of V^{2+} and $V^{+\cdot}$, respectively (figure 1(B)). The stripes are not uniform. Bright and dark contrast patterns alternate. Individual domains are anisotropic and rather small. Their size ranges typically between 10 and 20 nm. Neighbouring domains with sharp boundaries are mutually rotated by multiples of 120°, indicating registry with the underlying hexagonal substrate surface. High-resolution experiments (figure 1(C)) reveal details of the molecular adlayer. Rows of bright dots are separated by parallel rows of dark-grey and light-grey ellipsoidal-like segments. The latter are tilted by $(60 \pm 5)°$ with respect to the main row direction. A cross-section analysis reveals that parallel rows of the same type are separated by (2.4 ± 0.2) nm for HS-5V5-SH. The periodicity between identical features within one row is estimated to be (0.50 ± 0.05) nm ($=\sqrt{3}a_{Au}$). In analogy to the comprehensive analysis of the low-coverage HS-6V6-SH adlayer reported in [17] we assign the dark rows to the positions of the alkyl chains in a fully extended all-trans conformation with the molecular axis parallel to the surface plane. The grey rows are attributed to the viologen moieties. The intermolecular distance of 0.43 nm ($=\sqrt{3}a_{Au} \sin 60°$) is too small to allow a plane-parallel alignment to the substrate, but also too large for a perfect stacking structure. This enables the two pyridyl rings to be slightly rotated with respect to each other. The bright dots are assigned to the positions of the terminal sulfur functionalities. We notice that infrared studies indicate co-adsorption of ClO_4^- ions into the viologen adlayer [17]. Based on crystallographic studies, the latter promotes a slightly tilted or twisted conformation of the two pyridyl rings [36]. Unfortunately, we were not able to resolve the location of the ClO_4^- ions in the present *in situ* STM study. Using the vectors of the primitive gold lattice, a_{Au} and b_{Au} (figure 1(E)), with $|a_{Au}| = |b_{Au}| = 0.2885$ nm as a basis, we propose the following commensurate unit cell in matrix notation $\begin{pmatrix} a \\ b \end{pmatrix} = \begin{pmatrix} 8 & 1 \\ -1 & 2 \end{pmatrix} \begin{pmatrix} a_{Au} \\ b_{Au} \end{pmatrix}$, which gives rise to $|a'| = 2.46$ nm, $|b'| = 0.5$ nm enclosing an angle $\alpha' = 83.3°$. The corresponding unit cell contains one HS-5V5-SH molecule. Both alkyl chains are aligned with one of the densely packed substrate directions (for instance $[1\bar{1}0]$), and the sulfur anchor group being tentatively placed in three-fold hollow sites. The co-adsorbed ClO_4^- ions are assumed to be localized next to the pyridyl rings of the respective viologen moieties. The area per molecule is obtained as $A_L(\text{STM}) = 1.22$ nm^2, which corresponds to a coverage of $\Gamma_L(\text{STM}) = 1.36 \times 10^{-10}$ mol cm^{-2}. This value is in good agreement with $\Gamma_L(\text{CV}) = (1.2 \pm 0.2)\ 10^{-10}$ mol cm^{-2} obtained from cyclic voltammetric experiments at low coverages. A similar analysis was carried out for all low-coverage adlayers of HS-*n*V*n*-SH. The respective unit cells are rather similar, except that the $|a'|$ distance increases by 0.2885 nm, i.e. one gold lattice constant, with each additional two CH_2 groups. Characteristic properties are summarized in table 1.

3.2. Single molecule junction conductance

3.2.1. Conductance traces. Employing an *in situ* STM/STS configuration, we recorded the current–distance characteristics to explore the electron transport properties of single molecule junctions Au(T)/HS-*n*V*n*-SH/Au(S) in an electrochemical environment. We aim at addressing the fundamental questions (i) how does the molecular conductivity change by tuning the redox state of the molecule (the 'electrolyte gate') and (ii) what is the influence of the alkyl chain length on the transport characteristics. We have chosen low-coverage as well as high-coverage HS-*n*V*n*-SH adlayers immobilized on Au(111)-(1 × 1) and a polyethylene-coated, viologen-free gold tip.

Typical retraction or pulling curves for HS-5V5-SH on Au(111)-(1 × 1) are shown in figure 2(A) at $E_S = -0.65$ V and $E_T = -0.55$ V. We observed three types of transient curve.

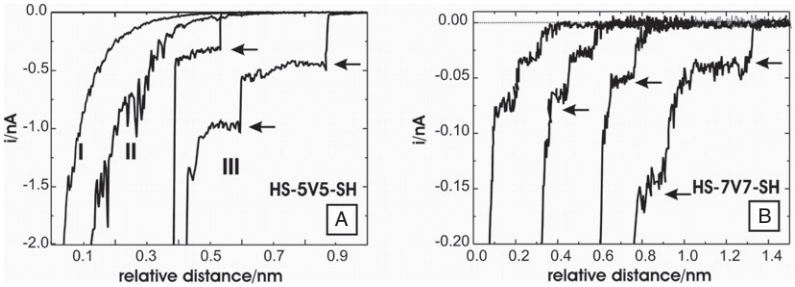

Figure 2. (A) Different types of current–distance curves recorded with a gold STM tip, coated with polyethylene, except for the very end of the apex, for HS-5V5-SH on Au(111)-(1 × 1) in 0.05 M $KClO_4$, pH ∼ 7, at $E_S = -0.65$ and $E_{bias} = 0.10$ V. The setpoint current before disabling the feedback was chosen at $i_o = 100$ pA. (B) Current–distance 'stretching' curves for molecular wires of HS-7V7-SH. Other conditions are identical with (A).

Type-I curves are characterized by a smooth experimental decay due to electron tunnelling between the gold tip and the substrate. No molecular junctions are formed. The percentage of these decay curves was 50% when starting with a high-coverage adlayer, and up to 70% for the striped, low-coverage phase of HS-5V5-SH. In both cases no viologen derivatives are present in the electrolyte phase. Type-II curves are noisy and non-monotonic, which could be attributed to mechanical vibrations, acoustic noise or impurities [37]. The percentage of these curves was around 10%. Traces of type I and type II were rejected when constructing the conductance histograms. Type-III conductance traces are monotonic and non-exponential. They exhibit a single plateau or a series of plateaus with a typical length of 0.05 to 0.2 nm, which are separated by abrupt steps. The corresponding currents are rather low and cannot be ascribed to the well-known quantization of a metal nanowire [28]. Instead, we assign the current steps to the breaking of individual respective multimolecular junctions previously formed between the gold STM tip and the substrate surface. This hypothesis is supported by the observations that these steps in current–distance traces are rarely (<2%) observed for the bare electrolyte as well as in experiments with HS-*n*V*n*-H, e.g. viologen-type monothiols capable of forming a chemical bond only to one of the adjacent gold electrodes. The percentage of type-III conductance traces varied between 40% and 20% for the high-coverage and the low-coverage HS-5V5-SH adlayers, respectively.

Similar data were obtained for the other Au(T)/HS-*n*V*n*-SH/Au(S), $n = 5$ to 8, junctions in an electrochemical environment. Figure 2(B) illustrates representatively a set of type-III transient conductance traces for HS-7V7-SH at $E = -0.65$ V, e.g. for the radical cation state. The noise level upon breaking a single molecular junction at $i \leqslant 3$ pA represents the current resolution of the experiments described in this paper.

3.2.2. Histograms. The statistical analysis of individual type-III conductance traces was carried out by constructing histograms, typically based on more than 500 measurements. Two strategies were chosen. The first approach is based on the selection of plateau currents applying the following criteria: minimum plateau length of 0.05 nm and an average variation of the current of less than 5%. Each plateau is represented by a single value of the corresponding conductance current. The histograms for HS-5V5-SH and HS-7V7-SH at $E_S = -0.65$ V and $E_{bias} = 0.1$ V are plotted in figures 3(A) and (C). Both graphs show a characteristic series of equally spaced current

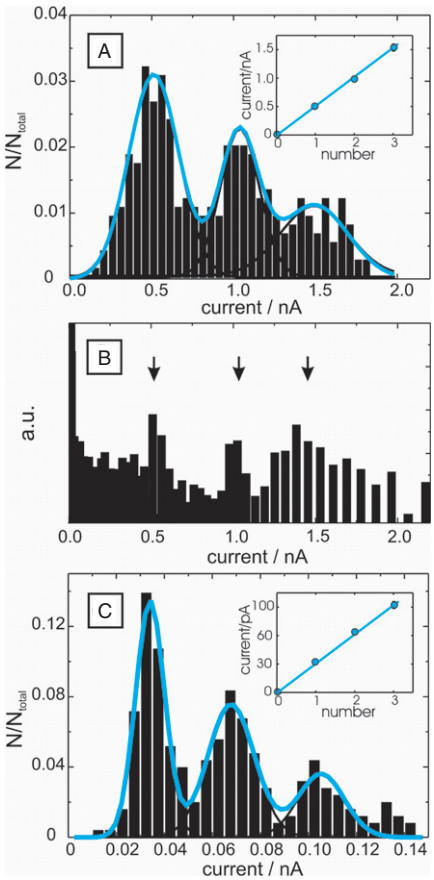

Figure 3. (A) Histogram constructed from values of the plateau current for HS-5V5-SH on Au(111)-(1 × 1) in 0.05 M $KClO_4$, pH ∼ 7, at $E_S = -0.65$ V, $E_{bias} = 0.10$ V. A total of 335 type-III 'stretching' curves out of 1100 total current–distance curves were selected; the bin width was 0.05 nA. The solid black and blue/pale grey lines represent the Gaussian fit. (B) Histogram based on a logarithmic analysis of the complete set of 335 type-III current–distance traces (see text for details). (C) Histogram constructed from values of the plateaus of current–distance traces of type III for HS-7V7-SH. The data base consists of 252 selected curves out of 1000. Other conditions are identical to (A). The insets in (A) and (C) show the dependences between the number of contacting molecules and the junction conductance.

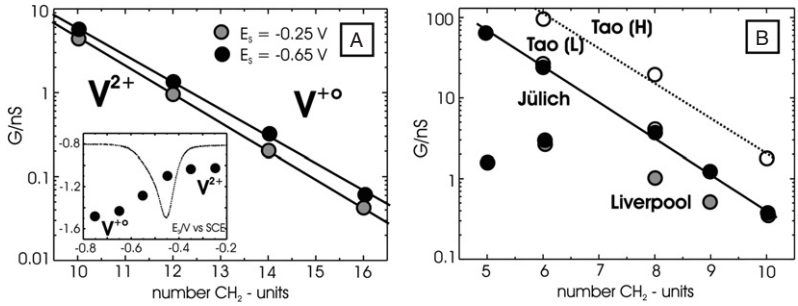

Figure 4. (A) Chain length dependence of the single junction conductivity Au(T)/HS-*n*V*n*-SH/Au(S), $n = 5$–8, in 0.05 M $KClO_4$, pH $\sim$ 7, for the oxidized V^{2+} and the reduced $V^{+\cdot}$ state of the viologen moiety. The inset illustrates the substrate potential dependence of the single junction conductance for HS-6V6-SH at fixed bias voltage $E_{bias} = 0.10$ V. Each data point was obtained from a statistical analysis of the plateau currents of type-III stretching curves. The dotted line represents the corresponding cathodic half-cycle of a voltammogram on a macroelectrode. (B) Chain length dependence of the single junctions conductance Au(T)/HS-C_m-SH/Au(S), $E_{bias} = 0.10$ V, for data obtained in this work (black symbols). For comparison, the data from Tao *et al* (white symbols [37]) and Haiss *et al* (grey symbols [45]) are added.

peaks, which represent one, two or three molecular junctions in the gap. The first peaks in these plots are attributed to the conductance current of single molecular junctions, which, under the particular experimental conditions, amount to (522 ± 20) pA for HS-5V5-SH and (35 ± 4) pA for HS-7V7-SH junctions in the radical cation state. Referring to the bias voltage of 0.10 V one obtains the corresponding single junction conductivities of (5.2 ± 2.0) nS and of (0.35 ± 0.04) nS.

The second approach to construct histograms is based on a recently proposed logarithmic analysis of the entire set of complete type-III conductance traces [38]. The first step comprises the construction of histograms choosing a bin width of 0.05 in the ln i scale, followed by the subtraction of the electron tunnelling contribution as well as of the digital noise in the low-current limit $i \to 0$. This procedure is accomplished by comparing histograms obtained with an identical number of simultaneously acquired type-I and type-III current–distance traces. The resulting curve was obtained after back-conversion into a linear current scale while keeping the bin width of the logarithmic representation. An example is plotted in figure 3(B) for HS-5V5-SH. The plot shows two characteristic conductance current maxima, which are in agreement with the results of the linear analysis, based on the above plateau selection criteria. However, two distinct differences shall be noticed: the graphs in figure 3(B) exhibit pronounced first and second conductance peaks and a broad higher-order feature. One also observes a significantly higher 'offset current', which might be attributed to the overall noise level and instability of the junction formed. These contributions are reduced in the first (linear) approach by extracting single plateau currents, while the latter, more robust and less selective approach treats the entire experimental transient without superimposing additional selection criteria. In consequence, one may state that the logarithmic analysis is less subjective and more general. However, agreement of the results for both approaches, as is demonstrated by comparing the plots in figures 3(A) and (B) for HS-5V5-SH junctions, gives confidence to the reliability of our histogram analysis strategy.

3.2.3. Potential and chain length dependence of viologen-based single molecule junctions. The above experiments were extended to substrate potentials in -0.70 V $\leqslant E_S \leqslant -0.20$ V for a series of N,N'-bis(n-thioalkyl)-4,4′-bipyridinium bromide (HS-*n*V*n*-SH) derivatives with $n = 5$ to 8. Several bias voltages $|E_{bias}| = |E_S - E_T| \leqslant 0.20$ V were tested. The statistical analysis of the individual conductance traces was carried out according to both approaches described above. The obtained conductivities of single junctions Au(T)/HS-*n*V*n*-SH/Au(S) are plotted in figure 4(A) for $E_S = -0.25$ V and $E_S = -0.65$ V, e.g. the viologen dication V^{2+} and the corresponding radical cation $V^{+\cdot}$ states. The numerical results are summarized in table 2. The single junction conductance of the 'reduced' radical cation state is approximately 50% higher than the corresponding 'oxidized' dication state. The inset in figure 4(A) illustrates the substrate potential dependence of the single junction conductance for Au(T)/HS-6V6-SH/Au(S), $E_{bias} = 0.10$ V. The conductance is rather constant in the stability range of the oxidized viologen dication V^{2+}, increases at substrate potentials <-0.40 V, and reaches a plateau at $E_S \leqslant -0.70$ V, e.g. past the formal potential of the reversible one-electron redox process leading to the stable radical cation state $V^{+\cdot}$. We tentatively attribute the sigmoid increase of the molecular conductance current to the higher electron density and the higher conjugation of the radical cation molecular wire as compared to the dication bridge. This view is supported by force field calculations of Hesters *et al* [41]. These authors reported that the interring bond order increases when the viologen dication transforms into the radical upon reduction, which implies that the aromatic character extends across both rings for the latter.

Table 2. Single junction conductance data (in nS) for the oxidized (V^{2+}, $E_S = -0.25$ V) and the reduced state ($V^{+\cdot}$, $E_S = -0.65$ V) of Au(T)/HS-*n*V*n*-SH/Au(S) junctions in 0.05 M $KClO_4$, pH $\sim$ 7, at two selected potentials.

*n*V*n*	5	6	7	8
V^{2+}	3.90 ± 0.10	1.00 ± 0.02	0.21 ± 0.01	0.040 ± 0.001
$V^{+\cdot}$	5.22 ± 0.12	1.43 ± 0.03	0.34 ± 0.01	0.060 ± 0.002

The values of the conductance of the single junctions Au(T)/HS-*n*V*n*-SH/Au(S) are similar to bridges of carotene-type molecules having a highly conjugated backbone [42],

and are significantly higher than alkanedithiol wires of comparable chain length [37, 43]. The logarithmic plots of the conductance G versus the number of CH_2-units are linear for both oxidation states and follow the simple tunnelling model with $G = G_{con}\exp(-\beta_N N)$, where β_N is the decay constant and the pre-exponential factor G_{con} is related to the metal/molecule contacts. β_N represents a characteristic parameter to classify the ability of (single) molecular junctions to facilitate tunnelling and to extract details of the electron transfer [4, 39, 40]. The parameters β_N and G_{con} were estimated as (0.76 ± 0.13) and (9 ± 2) μS for the viologen dication V^{2+}, and (0.74 ± 0.13) and (10 ± 4) μS for the radical cation $V^{+\cdot}$. With the typical length contributions of 0.125 nm per CH_2-group in an all-trans alkyl chain one obtains $\beta_{CH2} = (5.9\text{–}6.1)$ nm^{-1}. These data are compared in figure 4(B) with values of the single junction conductance of a series of alkanedithiols HS-C_m-SH. The experimental protocol followed the strategy outlined in section 2.4. Within the error limit, identical single molecule conductance values were obtained under electrochemical conditions in 0.05 M $KClO_4$ as well as in mesitylene (1,3,5-trimethylbenzene) or in oxygen-free argon atmosphere for bias voltages $|E_{bias}| \leqslant 0.20$ V [43]. We point out that our data are in agreement with the low-conductance data recently reported by Tao (Tao (L)) [37] in toluene, and with UHV data for alkanedithiols in an asymmetric bridge (hollow) site/atop configuration forming an extended all-trans chain [44]. However, except for a second set of single molecule conductance data for C_5 and C_6, our values are typically higher than the results published by the Liverpool group (Haiss [45]). A comprehensive analysis of our experiments with Au(T)/HS-C_m-SH/Au(S) junctions and a detailed comparison with published data obtained by different STM-type approaches will be given elsewhere [43].

Here we will focus on the chain length dependence of the conductance in Au(T)/HS-C_m-SH/Au(S) junctions. The data plotted in figure 4(B) follow the tunnelling model with $\beta_C = (1.03 \pm 0.30)$, respectively $\beta_{CH2} = (8.2 \pm 0.2)$ nm^{-1}, and $G_{con} = (9.5 \pm 0.2)$ μS. These β-values are in good agreement with data reported for tunnelling through saturated alkanedithiol chains (cf [37, 40, 46]). The decay constant β_C (β_{CH2}) for single alkandithiol junctions (figure 4(B)) is significantly higher than the value obtained for the redox-active viologens with variable alkyl chain length (figure 4(A)). The values of G_{con} scatter around 10 μS for both systems, and are rather independent of the redox state of the viologens. Comparing Au(T)/HS-nVn-SH/Au(S) and Au(T)/HS-C_m-SH/Au(S) junctions with the same number of CH_2-units, e.g. $m = 2n$, as derived from the data plotted in figure 4, one deduces that the single molecule conductance of the former is one to two orders of magnitude larger than the latter, and that this difference increases with increasing chain length. In an attempt to rationalize this result we assume that the single molecule conductance of the two types of junction, $G_{HS\text{-}Cm\text{-}SH}$ and $G_{HS\text{-}n\mathrm{V}n\text{-}SH}$, is given by the following expressions [44, 47]:

$$G_{HS\text{-}Cm\text{-}SH} = T_{conT} \cdot T_{Cm} \cdot T_{conS} \cdot G_o \qquad (1)$$

$$G_{HS\text{-}n\mathrm{V}n\text{-}SH} = T_{conT} \cdot T_{Cn} \cdot T_{BP} \cdot T_{Cn} \cdot T_{conS} \cdot G_o. \qquad (2)$$

Here, T_{conT}, T_{Cm} and T_{conS} represent the transmission functions for the contacts between the Au tip and the alkyl chain (Au(T)/–S–/C_m), and the alkyl chain (–S–/C_m/–S–) as well as the contact between the alkyl chain and the substrate (C_m/–S–/Au(S)). The viologen-type junction requires two additional terms representing the transmission functions of the bipyridyl moiety T_{BP} (–CH_2–/BP/–CH_2–) and of the alkyl chains between the sulfur and the pyridyl functionality, T_{Cn} (–S–/$(CH_2)_n$/–BP). $G_o = 77$ μS is the quantum conductance. The contributions of T_{conT} and T_{conS} are expected to be similar for both junctions because they represent identical Au–S bonds, and the sulfurs are attached to saturated alkyl chains. In this context we notice that the values of the contact conductance in electrolyte are higher (~10 μS, this work) than those reported under UHV conditions (~3 μS [44]). The conductance contribution of T_{Cm} appears to decrease more rapidly with increasing number of CH_2-units than $T_{Cn}\cdot T_{BP}\cdot T_{Cn}$. We propose two hypotheses to rationalize this trend. (i) First, the presence of the viologen moiety suppresses gauche defects and facilitates an all-trans conformation of the alkyl chains, which is known to exhibit a higher conductance [44]. (ii) Second, the increasing length of the symmetrically arranged alkyl side chains might impose a gradual increasing, preferential coplanar alignment of the two pyridyl rings, which also enhances the conductance [40]. These issues are currently being explored in quantum chemical transport calculations.

4. Summary and conclusions

We have investigated the assembly and macroscopic redox properties of N,N'-bis(n-thioalkyl)-4,4′-bipyridinium bromide on Au(111)-(1 × 1) in 0.05 M $KClO_4$, pH ~ 7. Three different adlayer phases were found for HS-nVn-SH, a low-coverage disordered and a low-coverage striped phase of flat oriented molecules, and a high-coverage phase of upright or slightly tilted molecules. Using the primitive gold lattice as a basis one could represent the commensurate HS-5V5-SH striped phase in matrix notation by $\begin{pmatrix} a \\ b \end{pmatrix} = \begin{pmatrix} 8 & 1 \\ -1 & 2 \end{pmatrix}\begin{pmatrix} a_{Au} \\ b_{Au} \end{pmatrix}$. The length of the nearly rectangular unit cell increases with increasing length of the alkyl chains by 0.2885 nm per two CH_2-units.

Three types of conductance trace were observed: exponential ones (I), non-monotonic and noisy curves (II) as well as monotonic step-like ‘stretching’ curves (III). The latter were chosen for the statistical analysis to extract single junction conductance properties. The single junction conductance of N,N'-bis(n-thioalkyl)-4,4′-bipyridinium bromide in the reduced radical cation state is approximately 50% larger than in the dication state. The conductance decreases exponentially with the length of the CH_2 spacer units giving rise to a tunnelling decay constant of $\beta_{CH2} = 5.9\text{–}6.1$ nm^{-1}. Comparing Au(T)/HS-nVn-SH/Au(S) and Au(T)/HS-C_m-SH/Au(S) junctions with the same number of CH_2-units, e.g. $m = 2n$, one deduces that the single molecule conductance of the former is one to two orders of magnitude larger than the latter, and that this difference increases with increasing chain length. The difference is attributed to conformational changes between these junctions. The contact conductance was estimated as 10 μS for both types of molecular junction investigated.

The proposed experimental method and data analysis represent a robust and reliable strategy for exploring electron

transport phenomena at the single molecular level at electrified solid/liquid interfaces. The approach is also applicable to *ex situ* and ambient conditions. The custom design of molecular junctions offers fascinating opportunities for exploring correlations between junction structure and electron transport characteristics under a wide range of conditions including electrical, mechanical, optical or temperature excitations as well as their combinations.

Acknowledgments

This work was supported by the Volkswagen Foundation, the HGF Project 'Molecular Switches', IFMIT and the Research Center Jülich. IP acknowledges support of the German Academic Exchange Agency for a PhD fellowship.

References

[1] Aviram A and Ratner M 1974 *Chem. Phys. Lett.* **29** 277
[2] Joachim C, Gimzewski J K and Aviram A 2000 *Nature* **408** 541
[3] Mantooth B and Weiss P S 2003 *Proc. IEEE* **91** 1785
[4] Adams D M *et al* 2003 *J. Phys. Chem.* B **107** 6668
[5] McCreery R L 2004 *Chem. Mater.* **16** 4477
[6] Szuchmacher-Blum A, Kushmerick J G, Long D P, Patterson C H, Yang J C, Henderson J C, Yao Y, Tour J M, Shashidhar R and Ratna B R 2005 *Nat. Mater.* **4** 167
[7] Molecular wires and nanoscale conductors *Faraday Discuss.* 2006 vol 131 (RSC Publishing)
[8] Di Ventra M, Lang N D and Pantelides S T 2002 *Chem. Phys.* **281** 189
[9] White H S, Kittlesen G P and Wrighton M S 1984 *J. Am. Chem. Soc.* **106** 5375
[10] He H X, Zhu J, Tao N J, Nagahara L A, Amlani I and Tsui R 2001 *J. Am. Chem. Soc.* **123** 7730
[11] Meulenkamp E A 1999 *J. Phys. Chem.* B **103** 7831
[12] Krüger M, Buitelaar M R, Nussbaumer T M, Schönenberger C and Forro L 2001 *Appl. Phys. Lett.* **78** 1291
[13] Rosenblatt S, Yaish Y, Park J, Gore J, Sazonova V and McEuen P L 2002 *Nano Lett.* **2** 869
[14] Tao N J 1996 *Phys. Rev. Lett.* **76** 4066
[15] Gittins D I, Bethell D, Schiffrin D J and Nichols R J 2000 *Nature* **408** 67
[16] Haiss W, van Zalinge H, Higgins S J, Bethell D, Höbenreich H, Schiffrin D J and Nichols R J 2003 *J. Am. Chem. Soc.* **125** 15294
[17] Li Z, Han B, Meszaros G, Pobelov I, Wandlowski Th, Błaszczyk A and Mayor M 2006 *Faraday Discuss.* **131** 121
[18] Chi Q, Farver O and Ulstrup J 2005 *Proc. Natl Acad. Sci.* **102** 16203
[19] Alessandrini A, Salerno M, Frabboni S and Facci P 2005 *Appl. Phys. Lett.* **86** 133902
[20] Xu B, Xiao X, Yang X, Zang L and Tao N J 2005 *J. Am. Chem. Soc.* **127** 2386
[21] Xiao X, Nagahara L A, Rawlett A M and Tao N J 2005 *J. Am. Chem. Soc.* **127** 9235
[22] Albrecht T, Guckian A, Ulstrup J and Vos J G 2005 *Nano Lett.* **5** 1451
[23] Albrecht T, Moth-Poulsen K, Christensen J B, Hjelm J, Bjornholm Th and Ulstrup J 2006 *J. Am. Chem. Soc.* **128** 6574
[24] Xiao X, Brune D, He J, Lindsay S, Gorman C B and Tao N J 2006 *Chem. Phys.* **326** 138
[25] Xu B Q, Li X L, Xiao X Y, Sakaguchi H and Tao N J 2005 *Nano Lett.* **5** 1491
[26] Chen F, He J, Nuckolls C, Roberts T, Klare J E and Lindsay S 2005 *Nano Lett.* **5** 503
[27] Chen F, Nuckolls C and Lindsay S M 2006 *Chem. Phys.* **324** 236
[28] Xu B and Tao N J 2003 *Science* **301** 1221
[29] Bird C L and Kuhn A T 1981 *Chem. Soc. Rev.* **10** 49
[30] Alvarado R J, Mukherjee J, Pacsial E J, Alexander D and Raymo F M 2005 *J. Phys. Chem.* B **109** 6164
[31] Chen S and Deng F 2002 *Langmuir* **18** 8942
[32] De Long H C and Buttry D A 1990 *Langmuir* **6** 1319
De Long H C and Buttry D A 1992 *Langmuir* **8** 2491
[33] Sagara T, Kaba N, Komatsu M, Uchida M and Nakashima N 1998 *Electrochim. Acta* **43** 2183
[34] Tang X, Schneider Th and Buttry D A 1994 *Langmuir* **10** 2235
[35] Haiss W, van Zalinge H, Höbenreich H, Bethell D, Schiffrin D J, Higgins S J and Nichols R J 2004 *Langmuir* **20** 7694
[36] Polishchuk I Yu, Grineva L G, Polishchuk A P and Chernega A N 1996 *Zh. Obschei Khimii (Russ)* **66** 1530
[37] Li X, He J, Hihath J, Xu B, Lindsay S M and Tao N J 2006 *J. Am. Chem. Soc.* **128** 2135
[38] Gonzalez M T, Wu S, Huber R, van der Molen S J, Schönenberger Ch and Calame M 2006 *Nano Lett.* **6** 2238
[39] Bumm L A, Arnold J J, Dunbar T D, Allara D L and Weiss P S 1999 *J. Phys. Chem.* B **103** 8122
[40] Salomon A, Cahen D, Lindsay S, Tomfohr J, Engelkes V B and Frisbie C D 2003 *Adv. Mater.* **15** 1881
[41] Hester R E and Suzuki S 1982 *J. Phys. Chem.* **86** 4626
[42] He J, Chen F, Li J, Sankey O F, Terazono Y, Herrero Ch, Gust D, Moore T A, Moore A L and Lindsay S M 2005 *J. Am. Chem. Soc.* **127** 1384
[43] Pobelov I, Li Z, Wandlowski Th, Bagrets A and Evers F 2006 in preparation
[44] Fujihira M, Suzuki M, Fuji S and Nishikawa A 2006 *Phys. Chem. Chem. Phys.* **8** 3876
[45] Haiss W, Nichols R J, van Zalinge H, Higgins S J, Bethell D and Shiffrin D J 2004 *Phys. Chem. Chem. Phys.* **6** 4330
[46] Wang W, Lee T and Reed M A 2005 *Rep. Prog. Phys.* **68** 523
[47] Nitzan A 2001 *Ann. Rev. Phys. Chem.* **52** 681